

Consistency with continuity in conservative advection schemes for free-surface models

Edward S. Gross, Luca Bonaventura^{*,†} and Giorgio Rosatti

¹*Dipartimento di Ingegneria Civile ed Ambientale, Università degli Studi di Trento, Italy*

SUMMARY

The consistency of the discretization of the scalar advection equation with the discretization of the continuity equation is studied for conservative advection schemes coupled to three-dimensional flows with a free-surface. Consistency between the discretized free-surface equation and the discretized scalar transport equation is shown to be necessary for preservation of constants. In addition, this property is shown to hold for a general formulation of conservative schemes. A discrete maximum principle is proven for consistent upwind schemes. Various numerical examples in idealized and realistic test cases demonstrate the practical importance of the consistency with the discretization of the continuity equation. Copyright © 2002 John Wiley & Sons, Ltd.

KEY WORDS: free-surface flows; conservative schemes; advection equation; continuity equation; pollutant transport

1. INTRODUCTION

The analysis of the monotonicity properties of conservative numerical schemes for the scalar advection equation

$$\frac{\partial s}{\partial t} + \frac{\partial(us)}{\partial x} + \frac{\partial(vs)}{\partial y} + \frac{\partial(ws)}{\partial z} = 0 \quad (1)$$

has led to various sufficient conditions for monotonicity preservation, such as the total variation diminishing (TVD) property or l_1 contractivity (see for example the general reviews of these topics in References [1, 2]). However, these properties are often difficult or even impossible to prove for general multidimensional schemes. For example, the TVD property only extends to first-order, fully multidimensional schemes (see e.g. the results of Reference [3]). Therefore, in order to ensure some degree of monotonicity to multidimensional schemes used in applications, one-dimensional limiters are usually applied in each coordinate direction.

*Correspondence to: L. Bonaventura, Dipartimento di Ingegneria Civile ed Ambientale, Università Degli Studi di Trento, Mesiano di Povo, 38050 (TN), Italy.

†E-mail: bonavent@ing.unitn.it

Received 13 July 2000

Revised 3 April 2001

A minimal monotonicity requirement, which is, however, desirable of any numerical scheme for Equation (1), is that an initially uniform scalar field remains uniform in the absence of sources and sinks. This condition has been called the *constancy condition* in Reference [18], where it is also shown that instability can arise in methods in which it is violated. Although easily proven for most conservative schemes on domains with cell volumes that are constant in time, this property does not always follow for conservative discretizations of (1) coupled to free-surface flows. In fact, this property is granted if the conservative scheme employed is consistent with the discretization of the continuity equation. The concept of *consistency with continuity* has been discussed by various authors (see for example References [4–7]), especially in connection with the links of conservative schemes to their respective advective versions. A convenient definition is given in Reference [6]: *a discretization of the advection equation is consistent with continuity if, given a spatially uniform scalar field as an initial datum, and a general flow field, the discretized scalar advection equation reduces to the discretized continuity equation*. It is to be remarked that this definition applies whether or not the grid volumes vary in time and space. It is also to be noted that consistency with continuity plays a key role in the monotonicity proof presented in Reference [8] for an accurate advection scheme on unstructured grids.

The purpose of this paper is to present a discretization approach for the scalar transport equation coupled to free-surface flow that ensures the consistency with the semi-implicit discretization of the continuity equation proposed in References [9, 10]. When coupled to an Eulerian–Lagrangian treatment of momentum advection, this semi-implicit discretization yields highly efficient numerical methods that allow for high-resolution, long time range simulations at low computational cost. The resulting algorithms, also known as TRIM, have been widely applied to two- and three-dimensional shallow water models for hydraulics and estuarine simulations ([4, 9–12]) and have been recently extended also to unstructured grids and non-hydrostatic flows in References [13, 14]. For this practical reason it is important that advection schemes can be easily devised that are consistent with this discretization, so that computationally intensive, long time range simulations of pollutant or sediment transport can be carried out taking advantage of the very efficient TRIM methods. However, the concept of consistency with continuity is clearly relevant also for any other discretization. It is immediate to verify that consistency with continuity is a sufficient condition for the constancy condition. It will also be shown by one- and two-dimensional numerical tests with idealized problems that, if the consistency with continuity is violated, initially constant scalar fields may develop unphysical maxima, especially when the free-surface elevation changes abruptly. This is shown to occur even when monotone or TVD schemes are applied for the discretization of advection. The discrete maximum principle can be proven if the simplest form of the upwind scheme is applied so as to obtain discretizations that are consistent with the continuity discretization of TRIM. However, as soon as transverse fluxes are taken into account, the discretization is no longer CWC and, therefore, examples in which the discrete maximum principle fails can be easily produced. As an example, this is shown to be the case for the first order, multidimensional upwind methods proposed in References [5, 15], also known as Corner Transport Upwind scheme. Finally, realistic two- and three-dimensional simulations have been carried out with upwind advection schemes coupled to the TRIM method, in order to show that results obtained with non-consistent discretizations yield quite different and unphysical results with respect to consistent schemes.

2. SCALAR ADVECTION FOR FREE-SURFACE APPLICATIONS

An equation for the free-surface elevation, $\eta(x, y, t)$, above a reference, undisturbed water level is obtained by integrating the continuity equation over the water column and combining it with the kinematic boundary condition at the free-surface (see for example the derivation in Reference [10]). This yields

$$\frac{\partial \eta}{\partial t} + \frac{\partial}{\partial x} \left[\int_{-h}^{\eta} u \, dz \right] + \frac{\partial}{\partial y} \left[\int_{-h}^{\eta} v \, dz \right] = 0 \tag{2}$$

where $h(x, y)$ is the depth of the lower boundary measured from an undisturbed water level. Equation (2) reduces to the shallow-water continuity equation

$$\frac{\partial \eta}{\partial t} + \frac{\partial(UH)}{\partial x} + \frac{\partial(VH)}{\partial y} = 0 \tag{3}$$

where $U(x, y, t)$ and $V(x, y, t)$ are the vertically averaged horizontal velocity components and $H(x, y, t) = h(x, y) + \eta(x, y, t)$ is the total water depth. The scalar advection Equation (1) is not in a form directly useful in free-surface simulations, where the vertical grid spacing, Δz , changes in time as the free-surface moves. The appropriate formulation is given in this context by the layer-averaged advective transport equation for each layer k ,

$$\frac{\partial(s\Delta z)_k}{\partial t} + \frac{\partial(us\Delta z)_k}{\partial x} + \frac{\partial(vs\Delta z)_k}{\partial y} + (ws)_{k+1/2} - (ws)_{k-1/2} = 0 \tag{4}$$

(see Reference [11]). Here s denotes the concentration of the advected tracer. The notation $(f)_k$ indicates the layer-averaged value of f in layer k and $(g)_{k+1/2}$ indicates the value of g at the height corresponding to $k + 1/2$. Layer-averaging in the top layer and applying the kinematic boundary condition at the free-surface results in the equation

$$\frac{\partial(s\Delta z)_k}{\partial t} + \frac{\partial(us\Delta z)_k}{\partial x} + \frac{\partial(vs\Delta z)_k}{\partial y} - (ws)_{k-1/2} = 0 \tag{5}$$

When only one vertical layer is present, Equation (4) is equivalent to the vertically averaged scalar advection equation

$$\frac{\partial(SH)}{\partial t} + \frac{\partial(USH)}{\partial x} + \frac{\partial(VSH)}{\partial y} = 0 \tag{6}$$

where $S(x, y, t)$ is the vertically averaged scalar concentration.

3. THE DISCRETIZED CONTINUITY EQUATION

The free-surface Equation (2) has been discretized in Reference [10] on an Arakawa C-type staggered grid as follows:

$$\eta_{i,j}^{n+1} = \eta_{i,j}^n - \frac{\Delta t}{\Delta x} \left[\sum_{k=m}^M \Delta z_{i+1/2,j,k}^n u_{i+1/2,j,k}^{n+\theta} - \sum_{k=m}^M \Delta z_{i-1/2,j,k}^n u_{i-1/2,j,k}^{n+\theta} \right]$$

$$-\frac{\Delta t}{\Delta y} \left[\sum_{k=m}^M \Delta z_{i,j+1/2,k}^n v_{i,j+1/2,k}^{n+\theta} - \sum_{k=m}^M \Delta z_{i,j-1/2,k}^n v_{i,j-1/2,k}^{n+\theta} \right] \quad (7)$$

where Δx and Δy are the constant horizontal grid spacings, $m = m(i, j)$ and $M = M(i, j)$ denote the bottom and top computational cells for each water column; $\Delta z_{i,\pm 1/2,j,k}$ and $\Delta z_{i,j,\pm 1/2,k}$ are the heights of the flux faces. This discretization is locally and globally conservative. The time discretization method is the so-called *generalized trapezoidal* method, so that $u^{n+\theta} = \theta u^{n+1} + (1-\theta)u^n$ and the parameter θ takes values in $[1/2, 1]$ for stability of the semi-implicit TRIM method (see Reference [10]). The vertical velocity is determined by the discrete continuity equation:

$$w_{i,j,k+1/2}^{n+\theta} = w_{i,j,k-1/2}^{n+\theta} - \frac{\Delta z_{i+1/2,j,k}^n u_{i+1/2,j,k}^{n+\theta} - \Delta z_{i-1/2,j,k}^n u_{i-1/2,j,k}^{n+\theta}}{\Delta x} - \frac{\Delta z_{i,j+1/2,k}^n v_{i,j+1/2,k}^{n+\theta} - \Delta z_{i,j-1/2,k}^n v_{i,j-1/2,k}^{n+\theta}}{\Delta y} \quad (8)$$

At the bottom of the water column, $w_{i,j,m-1/2}^{n+\theta} = 0$. Whenever the free-surface does not cross the uppermost model layer, M is constant and $\Delta z_{i,j,M}^{n+1} - \Delta z_{i,j,M}^n = \eta_{i,j}^{n+1} - \eta_{i,j}^n$ and, in the case of a single vertical layer, Equation (7) reduces to a discretization of Equation (3).

Positivity of cell volumes is only ensured under appropriate conditions on the time step (see the discussion in Section 5). For practical use, wetting and drying of cells is taken into account as described in Reference [11]. With this treatment of wetting and drying, cells whose depth is smaller than a minimal threshold are marked as dry cells.

4. THE DISCRETIZED SCALAR ADVECTION EQUATION

In this section, appropriate formulations for discretizations of the layer-averaged Equation (4) are presented, which ensure the CWC property with respect to the discretized free-surface continuity Equation (7). Both one-step and splitting methods are outlined. It will be shown that several commonly used discretization approaches can be formulated along these lines.

In order for a one-step update to be consistent with the discretization of the continuity equation of the TRIM methods, the following general form is sufficient:

$$s_{i,j,k}^{n+1} \Delta z_{i,j,k}^{n+1} = s_{i,j,k}^n \Delta z_{i,j,k}^n - \frac{\Delta t}{\Delta x} \left(\Delta z_{i+1/2,j,k}^n u_{i+1/2,j,k}^{n+\theta} s_e - \Delta z_{i-1/2,j,k}^n u_{i-1/2,j,k}^{n+\theta} s_w \right) - \frac{\Delta t}{\Delta y} \left(\Delta z_{i,j+1/2,k}^n v_{i,j+1/2,k}^{n+\theta} s_n - \Delta z_{i,j-1/2,k}^n v_{i,j-1/2,k}^{n+\theta} s_s \right) - \Delta t \left(w_{i,j,k+1/2}^{n+\theta} s_u - w_{i,j,k-1/2}^{n+\theta} s_l \right) \quad (9)$$

In the top cell (i, j, M) in each water column, Equation (5) is discretized, thus resulting in

$$\begin{aligned}
 s_{i,j,M}^{n+1} \Delta z_{i,j,M}^{n+1} &= s_{i,j,M}^n \Delta z_{i,j,M}^n \\
 &- \frac{\Delta t}{\Delta x} \left(\Delta z_{i+1/2,j,M}^n u_{i+1/2,j,M}^{n+\theta} s_e - \Delta z_{i-1/2,j,M}^n u_{i-1/2,j,M}^{n+\theta} s_w \right) \\
 &- \frac{\Delta t}{\Delta y} \left(\Delta z_{i,j+1/2,M}^n v_{i,j+1/2,M}^{n+\theta} s_n - \Delta z_{i,j-1/2,M}^n v_{i,j-1/2,M}^{n+\theta} s_s \right) \\
 &+ \Delta t \left(w_{i,j,M-1/2}^{n+\theta} s_l \right)
 \end{aligned} \tag{10}$$

In the above formulas, interpolated values of the advected quantity at the cell faces have been used, denoted by s_e, s_w, s_n, s_s, s_u and s_l . The methods of space and time interpolation are intentionally not specified. Various interpolation methods and time levels (from explicit to fully implicit) can be used while maintaining consistency with continuity. The only property required of the interpolation method is that in the case of a uniform scalar field, ($s_{i,j,k}^o = s^o$, for all i, j, k in the computational domain) the interpolated value on all flux faces is equal s^o . This is true for the interpolation methods of commonly used numerical schemes, including first-order upwind, central difference, Lax–Wendroff, second-order upwind, flux limiting methods, etc. Furthermore, since conservative methods are being considered, *flux face uniqueness* is required, i.e. $(s_w)_{i,j,k} = (s_e)_{i-1,j,k}$, $(s_s)_{i,j,k} = (s_n)_{i,j-1,k}$ and $(s_l)_{i,j,k} = (s_u)_{i,j,k-1}$. It can be expected that Equation (9) is consistent with Equation (8) by noting that the indices of u, v, w and Δz are identical in the two equations. It will now be shown that, in a uniform scalar field, the discretization given by Equation (9) is equivalent to the discretized continuity Equation (8). This in turn ensures that an initially uniform scalar field remains uniform. Although this property can be proven in the most general case, for simplicity it will only be shown to hold for constant M (i.e., it will be assumed that the free-surface does not cross the uppermost model layer).

First, CWC will be illustrated for an arbitrary internal cell, i.e., one that is not intersected by the free-surface. An internal cell height is constant ($\Delta z_{i,j,k}^{n+1} = \Delta z_{i,j,k}^n$) in time. Assuming that $s_{i,j,k}^n = s^o$ for all i, j, k , Equation (9) can be written

$$\begin{aligned}
 s_{i,j,k}^{n+1} \Delta z_{i,j,k}^{n+1} &= s^o \left[\Delta z_{i,j,k}^n - \frac{\Delta t}{\Delta x} \left(\Delta z_{i+1/2,j,k}^n u_{i+1/2,j,k}^{n+\theta} - \Delta z_{i-1/2,j,k}^n u_{i-1/2,j,k}^{n+\theta} \right) \right. \\
 &- \frac{\Delta t}{\Delta y} \left(\Delta z_{i,j+1/2,k}^n v_{i,j+1/2,k}^{n+\theta} - \Delta z_{i,j-1/2,k}^n v_{i,j-1/2,k}^{n+\theta} \right) \\
 &\left. - \Delta t \left(w_{i,j,k+1/2}^{n+\theta} - w_{i,j,k-1/2}^{n+\theta} \right) \right]
 \end{aligned} \tag{11}$$

By substitution of Equation (8), Equation (11) can be simplified to

$$s_{i,j,k}^{n+1} \Delta z_{i,j,k}^{n+1} = s^o \Delta z_{i,j,k}^n \tag{12}$$

Therefore, $s_{i,j,k}^{n+1} = s^o$ and Equation (11) is equivalent to the discretized continuity Equation (8). The thickness of the top cell in each water column varies in time as the free-surface moves and, therefore, a more general proof of CWC is required. In the top cell ($k = M$), the scalar advection Equation (10), is

$$s_{i,j,M}^{n+1} \Delta z_{i,j,M}^{n+1} = s^o \left[\Delta z_{i,j,M}^n - \frac{\Delta t}{\Delta x} \left(\Delta z_{i+1/2,j,M}^n u_{i+1/2,j,M}^{n+\theta} - \Delta z_{i-1/2,j,M}^n u_{i-1/2,j,M}^{n+\theta} \right) - \frac{\Delta t}{\Delta y} \left(\Delta z_{i,j+1/2,M}^n v_{i,j+1/2,M}^{n+\theta} - \Delta z_{i,j-1/2,M}^n v_{i,j-1/2,M}^{n+\theta} \right) + \Delta t w_{i,j,M-1/2}^{n+\theta} \right] \quad (13)$$

Summation of the discretized continuity Equation (8) from ($k = m$) to ($k = M - 1$) results in

$$\Delta t w_{i,j,M-1/2}^{n+\theta} = -\frac{\Delta t}{\Delta x} \left[\sum_{k=m}^{M-1} \Delta z_{i+1/2,j,k}^n u_{i+1/2,j,k}^{n+\theta} - \sum_{k=m}^{M-1} \Delta z_{i-1/2,j,k}^n u_{i-1/2,j,k}^{n+\theta} \right] - \frac{\Delta t}{\Delta y} \left[\sum_{k=m}^{M-1} \Delta z_{i,j+1/2,k}^n v_{i,j+1/2,k}^{n+\theta} - \sum_{k=m}^{M-1} \Delta z_{i,j-1/2,k}^n v_{i,j-1/2,k}^{n+\theta} \right] \quad (14)$$

Substituting Equation (14) into Equation (13) results in

$$s_{i,j,M}^{n+1} \Delta z_{i,j,M}^{n+1} = s^o \left[\Delta z_{i,j,M}^n - \frac{\Delta t}{\Delta x} \left(\sum_{k=m}^M \Delta z_{i+1/2,j,k}^n u_{i+1/2,j,k}^{n+\theta} - \sum_{k=m}^M \Delta z_{i-1/2,j,k}^n u_{i-1/2,j,k}^{n+\theta} \right) - \frac{\Delta t}{\Delta y} \left(\sum_{k=m}^M \Delta z_{i,j+1/2,k}^n v_{i,j+1/2,k}^{n+\theta} - \sum_{k=m}^M \Delta z_{i,j-1/2,k}^n v_{i,j-1/2,k}^{n+\theta} \right) \right] \quad (15)$$

Furthermore, as long as the top cell has not become dry at time step $n + 1$, in which case the corresponding values of s need not to be updated, and considering that constant M has been assumed, $\Delta z_{i,j,M}^{n+1} - \Delta z_{i,j,M}^n = \eta_{i,j}^{n+1} - \eta_{i,j}^n$. Substituting Equation (7) into Equation (15) results in

$$s_{i,j,M}^{n+1} \Delta z_{i,j,M}^{n+1} = s^o \Delta z_{i,j,M}^{n+1} \quad (16)$$

which implies again $s_{i,j,k}^{n+1} = s^o$. Therefore, CWC and constancy preservation are assured for all i, j, k , whether cell i, j, k is an internal cell or a cell containing the free-surface.

For several applications, operator splitting schemes can also be convenient, since operator splitting allows any scheme that is stable in one dimension to be applied in two and three dimensions. It is possible to define a discretization of the advection equation based on operator splitting which is consistent with the free-surface discretization (Equation (7)). However, in order to maintain CWC, intermediate cell heights must be defined to be used in the intermediate scalar concentration updates. The scalar is advected first in the x direction

as follows:

$$\begin{aligned} \tilde{S}_{i,j,k}^n \Delta \tilde{z}_{i,j,k}^n = \\ s_{i,j,k}^n \Delta z_{i,j,k}^n - \frac{\Delta t}{\Delta x} \left(u_{i+1/2,j,k}^{n+\theta} \Delta z_{i+1/2,j,k}^n s_e - u_{i-1/2,j,k}^{n+\theta} \Delta z_{i-1/2,j,k}^n s_w \right) \end{aligned} \quad (17)$$

where the intermediate height $\Delta \tilde{z}^n$ is defined as

$$\Delta \tilde{z}_{i,j,k}^n = \Delta z_{i,j,k}^n - \frac{\Delta t}{\Delta x} \left(u_{i+1/2,j,k}^{n+\theta} \Delta z_{i+1/2,j,k}^n - u_{i-1/2,j,k}^{n+\theta} \Delta z_{i-1/2,j,k}^n \right) \quad (18)$$

The scalar is then advected in the y direction as follows:

$$\begin{aligned} \hat{S}_{i,j,k}^n \Delta \hat{z}_{i,j,k}^n = \\ \tilde{s}_{i,j,k}^n \Delta \tilde{z}_{i,j,k}^n - \frac{\Delta t}{\Delta y} \left(v_{i,j+1/2,k}^{n+\theta} \Delta \tilde{z}_{i,j+1/2,k}^n \tilde{S}_n - v_{i,j-1/2,k}^{n+\theta} \Delta \tilde{z}_{i,j-1/2,k}^n \tilde{S}_s \right) \end{aligned} \quad (19)$$

where the intermediate height $\Delta \hat{z}^n$ is defined as

$$\Delta \hat{z}_{i,j,k}^n = \Delta \tilde{z}_{i,j,k}^n - \frac{\Delta t}{\Delta x} \left(v_{i,j+1/2,k}^{n+\theta} \Delta \tilde{z}_{i,j+1/2,k}^n - v_{i,j-1/2,k}^{n+\theta} \Delta \tilde{z}_{i,j-1/2,k}^n \right) \quad (20)$$

The vertical scalar advection is then performed as follows:

$$s_{i,j,k}^{n+1} \Delta z_{i,j,k}^{n+1} = \hat{S}_{i,j,k}^n \Delta \hat{z}_{i,j,k}^n - \Delta t \left(w_{i,j,k+1/2}^{n+\theta} \hat{S}_u - w_{i,j,k-1/2}^{n+\theta} \hat{S}_l \right) \quad (21)$$

The operator splitting approach outlined may introduce directional bias. To eliminate directional bias and achieve higher time accuracy, the order in which the updates are performed can be alternated between successive time steps. The proof that this splitting scheme is consistent with continuity is analogous to the proof for the one-step method (Equation (9)). A splitting scheme of this type, employing an explicit time discretization in the horizontal and an implicit time discretization in the vertical, has been successfully applied to study scalar transport in an estuary with broad intertidal areas that experience wetting and drying during each tidal cycle in Reference [4].

5. DISCRETE MAXIMUM PRINCIPLE FOR THE CONSISTENT UPWIND DISCRETIZATION

In this section, the CWC condition is used in a proof of the discrete maximum principle for the upwind scheme applied to scalar advection coupled to a free surface flow. It will also be shown that this result does not hold for fully multidimensional first-order schemes, which take into account the fluxes in the transverse directions, unless far more restrictive time step restrictions that would depend on the gradients of total water depth are introduced. For clarity of the presentation, only the case of the vertically averaged equations will be discussed in detail, but analogous results can be proven for three-dimensional schemes.

Local Courant numbers are defined for conciseness as

$$c_{i+1/2,j}^x = \frac{\Delta t}{\Delta x} U_{i+1/2,j}^{n+\theta}$$

and their positive and negative parts are defined by

$$c_{i+1/2,j}^{x,+} = \frac{\Delta t}{2\Delta x} (U_{i+1/2,j}^{n+\theta} + |U_{i+1/2,j}^{n+\theta}|), \quad c_{i+1/2,j}^{x,-} = -\frac{\Delta t}{2\Delta x} (U_{i+1/2,j}^{n+\theta} - |U_{i+1/2,j}^{n+\theta}|)$$

so that $c_{i+1/2,j}^x = c_{i+1/2,j}^{x,+} - c_{i+1/2,j}^{x,-}$. The values of the corresponding quantities in the y are defined analogously.

Given these definitions, a free-surface version of the upwind scheme that is consistent with the discretized continuity Equation (7) of the TRIM method can be conveniently written as

$$\begin{aligned} S_{i,j}^{n+1} H_{i,j}^{n+1} &= S_{i,j}^n \left\{ H_{i,j}^n - H_{i+1/2,j}^n c_{i+1/2,j}^{x,+} + H_{i-1/2,j}^n c_{i-1/2,j}^{x,-} - H_{i,j+1/2}^n c_{i,j+1/2}^{y,+} + H_{i,j-1/2}^n c_{i,j-1/2}^{y,-} \right\} \\ &+ S_{i+1,j}^n H_{i+1/2,j}^n c_{i+1/2,j}^{x,-} + S_{i-1,j}^n H_{i-1/2,j}^n c_{i-1/2,j}^{x,+} \\ &+ S_{i,j+1}^n H_{i,j+1/2}^n c_{i,j+1/2}^{y,-} + S_{i,j-1}^n H_{i,j-1/2}^n c_{i,j-1/2}^{y,+} \end{aligned} \quad (22)$$

The discrete maximum principle is now proven in two steps. Positivity of the above scheme is proven first, under suitable conditions on the time-step. In order to prove positivity, it is sufficient to show that all the coefficients of the S values in the right hand side of Equation (22) are greater than or equal to zero. The only coefficient that may become negative is

$$H_{i,j}^n - H_{i+1/2,j}^n c_{i+1/2,j}^{x,+} + H_{i-1/2,j}^n c_{i-1/2,j}^{x,-} - H_{i,j+1/2}^n c_{i,j+1/2}^{y,+} + H_{i,j-1/2}^n c_{i,j-1/2}^{y,-} \quad (23)$$

For some definitions of H at the flux faces, requiring the sum in Equation (23) to be non-negative could result in exceedingly severe time-step restrictions. Here, the cell height at the center of the cell is naturally defined at each time step as

$$H_{i,j}^n = \max(0, h_{i,j} + \eta_{i,j}^n) \quad (24)$$

where $h_{i,j}$ is the depth of the lower boundary measured from an undisturbed water level. Along the lines of what was proposed in Reference [7], the flux face heights are then defined as

$$H_{i+1/2,j}^n = \max(0, h_{i+1/2,j} + \eta_{\text{upwind}}^n) \quad (25)$$

where, if $U_{i+1/2,j}^n \geq 0$ then $\eta_{\text{upwind}}^n = \eta_{i,j}^n$, and, if $U_{i+1/2,j}^n < 0$, then $\eta_{\text{upwind}}^n = \eta_{i+1,j}^n$. Using this definition of the $H_{i+1/2,j}^n$ it is immediate to see that, for any non-empty cell, the condition required for the positivity of Equation (23) is equivalent to

$$c_{i+1/2,j}^{x,+} - c_{i-1/2,j}^{x,-} + c_{i,j+1/2}^{y,+} - c_{i,j-1/2}^{y,-} \leq 1 \quad (26)$$

for all (i, j) . Therefore, positivity will hold, provided that this condition is satisfied. This Courant number restriction only involves the horizontal velocities and does not require any assumption on the values of H^n . Furthermore, condition (26) also implies that the water depths

H computed by the discrete continuity Equation (7) are non-negative. It is also to be remarked that this proof relies on the implicit assumption that the upwind directions determined by $U_{i+1/2,j}^n$ and $U_{i+1/2,j}^{n+0}$ are the same. However, due to the regularity of the flow fields considered, this is found to be generally true for estuarine applications when condition (26) holds.

Monotonicity follows then by the consistency of the numerical scheme with the discretized continuity equation and by arguments analogous to those made in Theorem 13.5.1 of Reference [2]. In fact, the CWC properties plays in this proof exactly the same role of the *flux consistency* condition usually required for conservation law schemes. More specifically, assume that positivity of the numerical solution $S_{i,j}^n$ is maintained at time $n + 1$. As it was shown before, inequality (26) is a sufficient condition for this to be true. Due to linearity and homogeneity of the numerical scheme and assuming the fluxes at the open boundaries to be equal to zero, positivity will then imply that, given two numerical solutions $S_{i,j}^n, T_{i,j}^n$ such that $S_{i,j}^n \leq T_{i,j}^n$ for all i, j in the computational domain, $S_{i,j}^{n+1} \leq T_{i,j}^{n+1}$. Taking then $T^n = \max_{i,j} S_{i,j}^n$ as initial datum at time step n , due to consistency with continuity it will follow that

$$T^{n+1} = T^n = \max_{i,j} S_{i,j}^n \geq S_{i,j}^{n+1}$$

By the same reasoning, the lower bound $\min_{i,j} S_{i,j}^n \leq S_{i,j}^{n+1}$ can also be proven, so that for a generic solution S it follows

$$\min_{i,j} S^n \leq S_{i,j}^{n+1} \leq \max_{i,j} S^n$$

6. EXAMPLES OF NON CONSISTENT AND NON MONOTONIC DISCRETIZATIONS

The CWC condition can be violated in a variety of ways: whenever the values of u, v, w and Δz used in the computation of the mass fluxes in Equation (9) do not coincide with the values at the cell sides that appear in Equation (7), the discrete continuity equation will not be recovered for the case of a constant initial datum. As previously noticed, employing a different discretization of the continuity equation, so as to yield CWC for a given advection scheme is not advisable, given the great computational advantages of the semi-implicit and mass conservative discretization (Equation (7)). For simplicity of the presentation, only discretizations of the vertically averaged two-dimensional equations will be now discussed in detail, but the same considerations apply to three-dimensional schemes and three-dimensional examples of the impact of the CWC condition will be presented in Section 8. For definiteness, two special cases of CWC violation will be considered in the following numerical comparisons. The first case is the discretization

$$\begin{aligned} S_{i,j}^{n+1} H_{i,j}^{n+1} &= S_{i,j}^n H_{i,j}^n \\ &- \frac{\Delta t}{\Delta x} \left(U_{i+1/2,j}^{n+1/2} (SH)_e - U_{i-1/2,j}^{n+1/2} (SH)_w \right) \\ &- \frac{\Delta t}{\Delta y} \left(V_{i,j+1/2}^{n+1/2} (SH)_n - V_{i,j-1/2}^{n+1/2} (SH)_s \right) \end{aligned} \tag{27}$$

Here, $(SH)_w, (SH)_e, (SH)_n, (SH)_s$ denote again values of the conserved quantity SH interpolated onto the sides of the computational cells. In the second case of a non-CWC scheme considered here, the velocity values U^{n+1}, V^{n+1} are used instead of the time averaged values employed in the continuity equation, so as to obtain

$$\begin{aligned}
 S_{i,j}^{n+1} H_{i,j}^{n+1} &= S_{i,j}^n H_{i,j}^n \\
 &- \frac{\Delta t}{\Delta x} \left(U_{i+1/2,j}^{n+1} H_{i+1/2,j}^n S_e - U_{i-1/2,j}^{n+1} H_{i-1/2,j}^n S_w \right) \\
 &- \frac{\Delta t}{\Delta y} \left(V_{i,j+1/2}^{n+1} H_{i,j+1/2}^n S_n - V_{i,j-1/2}^{n+1} H_{i,j-1/2}^n S_s \right)
 \end{aligned} \tag{28}$$

whereas the two-dimensional CWC scheme is given by

$$\begin{aligned}
 S_{i,j}^{n+1} H_{i,j}^{n+1} &= S_{i,j}^n H_{i,j}^n \\
 &- \frac{\Delta t}{\Delta x} \left(U_{i+1/2,j}^{n+1/2} H_{i+1/2,j}^n S_e - U_{i-1/2,j}^{n+1/2} H_{i-1/2,j}^n S_w \right) \\
 &- \frac{\Delta t}{\Delta y} \left(V_{i,j+1/2}^{n+1/2} H_{i,j+1/2}^n S_n - V_{i,j-1/2}^{n+1/2} H_{i,j-1/2}^n S_s \right)
 \end{aligned} \tag{29}$$

In the numerical tests described in the next sections, the results obtained by Equations (27), (28) and (29) will be compared using exactly the same interpolation procedure in both discretization schemes, so as to single out the effects of CWC violation. However, an example of the problems resulting from the use of Equation (27) can be given on a simple one-dimensional domain. In Figure 1 the simple geometry of the domain is depicted in profile

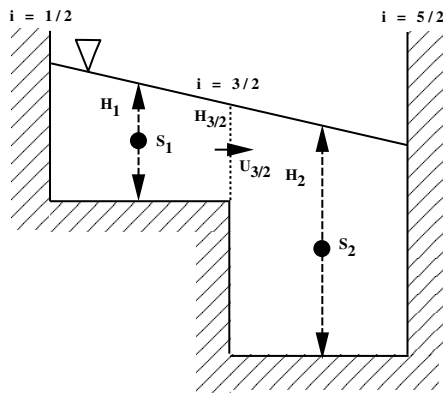


Figure 1. Violation of CWC on a two-cell grid.

view. The shaded area represents land and, therefore, the two grid cells in Figure 1 represent a closed system such as a lake. Initially the two grid cells have equal scalar concentrations $S_1^0 = S_2^0$ and different depths H_1^0, H_2^0 , respectively. The depth shown in Figure 1 varies between cells both due to varying water surface elevation and various depth from a constant vertical datum to the bottom. Because there is not water flux or scalar flux through the boundaries, flux of volume and scalar mass passes only through the interface of height $H_{3/2}^0$ between the two grid cells.

Using first-order upwind to interpolate the scalar concentration to the flux faces and assuming positive velocity, the discretization (Equation (27)) applied to this simple case yields for cell 1

$$(SH)_1^{n+1} = (SH)_1^n - \frac{\Delta t}{\Delta x} U_{3/2}^{n+1/2} (SH)_1^n \tag{30}$$

Substitution of Equation (7) for cell 1 results in

$$S_1^{n+1} \left(H_1^n - \frac{\Delta t}{\Delta x} U_{3/2}^{n+1/2} H_{3/2}^n \right) = S_1^n \left(H_1^n - \frac{\Delta t}{\Delta x} U_{3/2}^{n+1/2} H_1^n \right) \tag{31}$$

Thus, $S_1^{n+1} \neq S_1^n$ when $H_1^n \neq H_{3/2}^n$, so that, even in this very simple application, constant initial data are not preserved in general.

In order to show that, as far as CWC discretizations are concerned, the discrete maximum principle does not hold in general for schemes more sophisticated than simple upwind, the so called Corner Transport Upwind is considered, which was proposed in Reference [15] and has been reintroduced in a slightly different form in Reference [5]. This multi-dimensional scheme takes into account transverse flow in the computation of the upwind fluxes, thus resulting in a more accurate first-order scheme than the simplest multidimensional upwind.

The Courant–Friedrichs–Lewy condition (see References [1, 2]) for the CTU scheme is more relaxed, since it depends on the maximum of the Courant number in each coordinate direction. In the case of the discretization of the vertically averaged, two-dimensional advection Equation (6), the CTU scheme can be written as

$$\begin{aligned} S_{i,j}^{n+1} H_{i,j}^{n+1} &= S_{i,j}^n H_{i,j}^n \\ &- \left\{ H_{i+1/2,j}^n \left[c_{i+1/2,j}^{x,+} S_{i+1/2,j}^+ - c_{i+1/2,j}^{x,-} S_{i+1/2,j}^- \right] \right. \\ &- \left. H_{i-1/2,j}^n \left[c_{i-1/2,j}^{x,+} S_{i-1/2,j}^+ - c_{i-1/2,j}^{x,-} S_{i-1/2,j}^- \right] \right\} \\ &- \left\{ H_{i,j+1/2}^n \left[c_{i,j+1/2}^{y,+} S_{i,j+1/2}^+ - c_{i,j+1/2}^{y,-} S_{i,j+1/2}^- \right] \right. \\ &- \left. H_{i,j-1/2}^n \left[c_{i,j-1/2}^{y,+} S_{i,j-1/2}^+ - c_{i,j-1/2}^{y,-} S_{i,j-1/2}^- \right] \right\} \end{aligned} \tag{32}$$

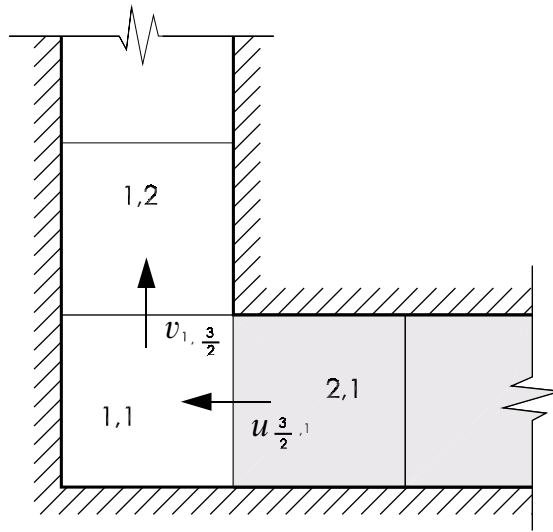


Figure 2. Counterexample to the discrete maximum principle for the free-surface CTU scheme.

where

$$S_{i+1/2,j}^+ = \left[S_{i,j}^n + \frac{c_{i,j-1/2}^{y,+}}{2} (S_{i,j-1}^n - S_{i,j}^n) - \frac{c_{i,j+1/2}^{y,-}}{2} (S_{i,j}^n - S_{i,j+1}^n) \right]$$

$$S_{i+1/2,j}^- = \left[S_{i+1,j}^n + \frac{c_{i+1,j-1/2}^{y,+}}{2} (S_{i+1,j-1}^n - S_{i+1,j}^n) - \frac{c_{i+1,j+1/2}^{y,-}}{2} (S_{i+1,j}^n - S_{i+1,j+1}^n) \right]$$

and the other analogous terms are defined accordingly. Here, the horizontal Courant numbers are defined as in the previous section. It can be easily noticed that this discretization is consistent with the continuity equation in the sense of the definition given the introduction. However, the discrete maximum principle does not hold for this scheme, as can be shown by the following example.

Consider a discretization grid representing an L-shaped channel as in Figure 2. In this plan view figure the shaded region is land and, therefore, the geometry is that of a channel one grid cell wide that bends at cell (1, 1). All velocities normal to the closed boundaries are taken to be zero, whereas an inflow from cell (2, 1) is assumed, so that $u_{3/2,1} < 0$ and $v_{1,3/2} > 0$. The CTU scheme update can be rewritten for cell (1, 1) as

$$S_{1,1}^{n+1} H_{1,1}^{n+1} = S_{1,1}^n H_{1,1}^n + H_{3/2,1}^n c_{3/2,1}^{x,-} S_{3/2,1}^- - H_{1,3/2}^n c_{1,3/2}^{y,+} S_{1,3/2}^+ \quad (33)$$

where:

$$S_{3/2,1}^- = S_{2,1}^n$$

$$S_{1,3/2}^+ = S_{1,1}^n - \frac{c_{3/2,1}^{x,-}}{2} (S_{1,1}^n - S_{2,1}^n)$$

This can be reformulated as

$$S_{1,1}^{n+1}H_{1,1}^{n+1} = S_{1,1}^n \left(H_{1,1}^n - H_{1,3/2}^n c_{1,3/2}^{y,+} + H_{1,3/2}^n \frac{c_{1,3/2}^{y,+} c_{3/2,1}^{x,-}}{2} \right) + S_{2,1}^n c_{3/2,1}^{x,-} \left(H_{3/2,1}^n - \frac{c_{1,3/2}^{y,+}}{2} H_{1,3/2}^n \right)$$

This shows that, assuming for example $S_{1,1}^n = 0$ and $S_{2,1} > 0$, a necessary condition for positivity of $S_{1,1}^{n+1}$ is

$$c_{1,3/2}^{y,+} \leq \frac{2H_{3/2,1}^n}{H_{1,3/2}^n}$$

Therefore, time-step restrictions involving total water depth ratios will be needed for this scheme to ensure positivity. This type of condition can be extremely restrictive and practically impossible to enforce for realistic applications, thus making the CTU effectively non-monotonic for realistic free-surface flows. However, it will be shown that in practice only very small non-monotonic effects are produced, even in simulations with realistic, complex bathymetry and real tides.

7. NUMERICAL TESTS: COMPARISON WITH ONE- AND TWO-DIMENSIONAL ANALYTICAL SOLUTIONS

Several numerical simulations have been carried out in order to estimate the effects of violating the CWC condition. In all the simulations, in order to avoid sources of numerical error other than the chosen advection scheme, the initial values for H, U was chosen as the appropriate value at the initial time for the analytical solution of the nonlinear shallow water equations considered in each case. The velocity field was then given at each time step by the analytical solution. The total water depth was computed by the discrete continuity Equation (7) and the scalar concentration field was finally updated with a conservative scheme using the previously computed values of H, U . In all the tests, a comparison has been carried out between the results obtained using schemes (29) and (27), respectively. Exactly the same procedures for reconstruction of the face values of S, SH were used in both discretization schemes, so as to single out the effects of CWC violation.

One-dimensional tests were performed with the analytical solution of the Riemann problem in the case of constant bottom depth (see, e.g., the derivation in Reference [16]). The initial value for H was taken to be a positive constant for $x \leq 0$ and 0 for positive values of x . The initial datum for S was assumed to be constant and equal to 1. In these simulations, cells with total depth less than 10^{-4} m were considered dry. The results obtained with a Lax–Wendroff slope limited TVD second-order scheme for reconstruction of the concentration values at the sides of the cell are displayed in Table I, where relative errors in l_1, l_2 norm and maximum and minimum values of the computed solution are shown after 50 time steps. Furthermore, a one-dimensional test with initial values for S given by a cosine pulse was also run. No new maxima are produced by the CWC slope limited second-order scheme, while the corresponding non-CWC scheme yields new maxima, as shown at various times in Table II. As expected, the largest errors are observed to occur at the edge of the wet area in all the above tests.

Table I. Results of one-dimensional simulation with constant initial datum, second-order TVD slope limited scheme.

	l_1	l_2	Maximum	Minimum
CWC	1.04e-8	5.84e-8	1.00	1.00
Non-CWC	6.25e-3	4.97e-2	1.07	3.16e-2

Table II. Maximum values in one-dimensional simulation with non-constant initial datum, second-order TVD slope limited scheme.

	10 time steps	20 time steps	30 time steps	40 time steps
CWC	0.99	0.99	0.99	0.99
Non-CWC	1.07	1.06	1.06	1.05

For two-dimensional tests, the analytical solutions given in Reference [17] by Thacker for oscillations in a parabolic basin were employed. An analytical solution to a vertically averaged, unsteady free-surface flow is used to specify the velocity field for various vertically averaged scalar advection discretizations. In this flow, the shoreline is not fixed and cells experience *wetting and drying* as the shoreline moves.

The governing equations of this test case are the shallow water equations for a constant density flow without bottom stress or horizontal diffusion but taking into account the Coriolis force.

$$\frac{\partial U}{\partial t} + U \frac{\partial U}{\partial x} + V \frac{\partial U}{\partial y} - fV + g \frac{\partial H}{\partial x} = 0 \quad (34)$$

$$\frac{\partial V}{\partial t} + U \frac{\partial V}{\partial x} + V \frac{\partial V}{\partial y} + fU + g \frac{\partial H}{\partial y} = 0 \quad (35)$$

$$\frac{\partial H}{\partial t} + \frac{\partial(UH)}{\partial x} + \frac{\partial(VH)}{\partial y} = 0 \quad (36)$$

where U and V are the horizontal velocity components in the x and y directions, respectively; g is the acceleration of gravity; f is the Coriolis parameter and $H = h + \eta$ is the depth. The bathymetry of the parabolic basin is described by the equation

$$h = h_{\text{cen}} \left(1 - \frac{x^2}{L^2} - \frac{y^2}{L^2} \right) \quad (37)$$

where $h(x, y)$ is the depth relative to the equilibrium free-surface level, h_{cen} is the depth at the center of the basin and x and y are zero at the center of the basin. L is the distance from the center of the basin to the circle of zero depth. The initial free-surface elevation at the center of the basin is η_{cen}^0 . The solution given by Thacker in Reference [17] is

$$U = \frac{1}{1 - A \cos(\omega t)} \left[\frac{1}{2} \omega x A \sin(\omega t) - \frac{1}{2} f y \left((1 - A^2)^{1/2} + A \cos(\omega t) - 1 \right) \right] \quad (38)$$

Table III. Results of two-dimensional simulation with constant initial datum, second-order scheme.

	l_1	l_2	Maximum	Minimum
CWC	5.44e-7	7.21e-7	1.00	1.00
Non-CWC	8.55e-3	4.13e-2	2.68	-5.48e-2

$$V = \frac{1}{1 - A \cos(\omega t)} \left[\frac{1}{2} \omega y A \sin(\omega t) + \frac{1}{2} f x \left((1 - A^2)^{1/2} + A \cos(\omega t) - 1 \right) \right] \tag{39}$$

$$\eta = h_{\text{cen}} \left(\frac{(1 - A^2)^{1/2}}{1 - A \cos(\omega t)} - 1 - \frac{x^2 + y^2}{l^2} \left[\frac{1 - A^2}{(1 - A \cos(\omega t))^2} - 1 \right] \right) \tag{40}$$

where A is given by

$$A = \frac{(h_{\text{cen}} + \eta_{\text{cen}}^0)^2 - h_{\text{cen}}^2}{(h_{\text{cen}} + \eta_{\text{cen}}^0)^2 + h_{\text{cen}}^2} \tag{41}$$

and ω is given by

$$\omega^2 = \frac{8gh_{\text{cen}}}{l^2} + f^2 \tag{42}$$

The analytical solution for η is used to specify the initial conditions and, η at all other times is computed using the discretized depth-averaged continuity equation.

$$\begin{aligned} \eta_{i,j}^{n+1} = \eta_{i,j}^n - \frac{\Delta t}{\Delta x} & \left[H_{i+1/2,j}^n U_{i+1/2,j}^{n+\theta} - H_{i-1/2,j}^n U_{i-1/2,j}^{n+\theta} \right] \\ & - \frac{\Delta t}{\Delta y} \left[H_{i,j+1/2}^n V_{i,j+1/2}^{n+\theta} - H_{i,j-1/2}^n V_{i,j-1/2}^{n+\theta} \right] \end{aligned} \tag{43}$$

The various parameters are selected to be representative of the geometry of many lakes and estuaries. The initial radius, L , is 12 km, the depth at the center of the basin, h_{cen} , is 10 m and the initial free-surface elevation at the center of the basin, η_{cen}^0 , is 0.5 m. The grid spacing is 100 m and the Coriolis parameter corresponds to a latitude of 56° . The time step is 6.72 s, and, therefore, one period of oscillation corresponds to 400 time steps.

Once again, an initially uniform scalar field is specified and the constancy of scalar concentration is tested for CWC and non-CWC discretization methods. First-order upwind interpolation is used for all two-dimensional simulations. In all cases, the free-surface height is computed using Equation (43) with $\theta = 1/2$. The initial datum for S was chosen to be constant and equal to 1. The Lax–Wendroff slope limited TVD second-order scheme reconstruction procedure was employed for the concentration values at the sides of the cell. In these simulations, cells with total depth less than 10^{-4} m were considered dry. The results obtained are displayed in Table III, where relative errors in l_1 , l_2 norm and maximum and minimum values of the computed solution are shown after 200 time steps, which correspond to half the period of the free-surface oscillations. Again, the largest errors occur in the areas

Table IV. Maximum values in two-dimensional simulation with non-constant initial datum, second-order scheme.

	30 time steps	60 time steps	90 time steps	120 time steps
CWC	1.00	1.00	1.00	1.00
Non-CWC	2.35	1.94	1.54	1.36

where wetting and drying occurs. Furthermore, a two-dimensional test with an initial datum for S given by a cosine hill was also run. No new maxima are produced by the second-order CWC scheme, while the corresponding non CWC scheme yields large new maxima, as shown at various simulation times in Table IV.

8. IMPORTANCE OF THE CWC CONDITION IN REALISTIC SIMULATIONS

The CWC methods outlined above have been applied to several realistic three-dimensional simulations of scalar transport in estuaries. Both the one-step update method and the splitting method have been used, along with velocities and free-surface elevations obtained by the hydrostatic TRIM method [10]. The simulation of discharge from a point source using a one-step update method is discussed in Reference [11]. Long-term salt transport is reproduced accurately in References [4, 12] using a splitting approach.

However, in order to measure the specific impact of the CWC violation also in realistic simulations characterized by strongly varying currents and complicated domain geometry, several two- and three-dimensional tests have been performed coupling the transport schemes to numerically simulated time-dependent dynamics obtained using the hydrostatic version of the TRIM method. The simulation domain was taken to be a high-resolution grid of the lagoon of Venice with $\Delta x = \Delta y = 50$ m. The schemes used for horizontal advection were:

1. the upwind, CWC scheme
2. the CTU, CWC scheme
3. the upwind, non-CWC scheme with wrong Δz (see, e.g., Equation (27))
4. the upwind, non-CWC scheme with wrong velocity (see, e.g., Equation (28)).

Firstly, two-dimensional simulations were performed starting from quiescent water and using constant initial and boundary values for the passive tracer concentration. Considering that about 12 h are needed for realistic flows to develop throughout the lagoon, a 24 h long simulation was run with real tidal elevation data as a boundary condition. The time step was taken to be 30s, which ensured that condition (26) was always satisfied. In Figure 3, relative errors of the upwind scheme 1 (with respect to the constant exact solution) in l_∞ , l_2 norm are reported as a function of time. It can be seen that average and peak values of the errors are very limited throughout the simulation. The key parameter which determines the order of magnitude of these errors for CWC schemes is the tolerance used in the preconditioned conjugate gradient algorithm for the implicit step. In fact, insufficient accuracy of the solution provided by the linear solver may induce numerical inconsistency between the fluxes evaluated implicitly in the system and those used in the advection computation. Relative errors in l_∞ , l_2 norm for the CTU scheme 2 in this test case coincide with the ones obtained for the upwind scheme up to

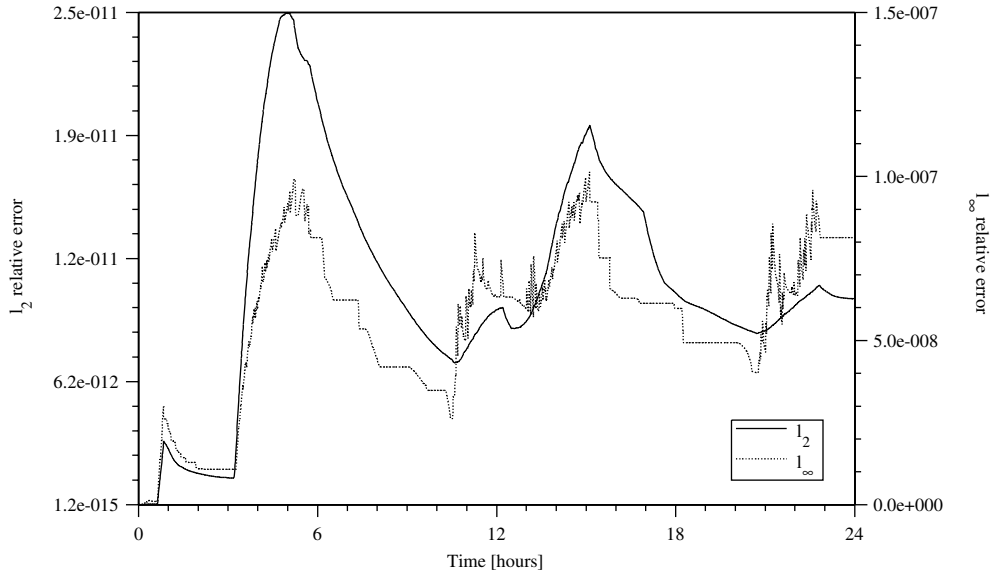


Figure 3. Relative errors for upwind CWC scheme 1, test case with uniform initial datum.

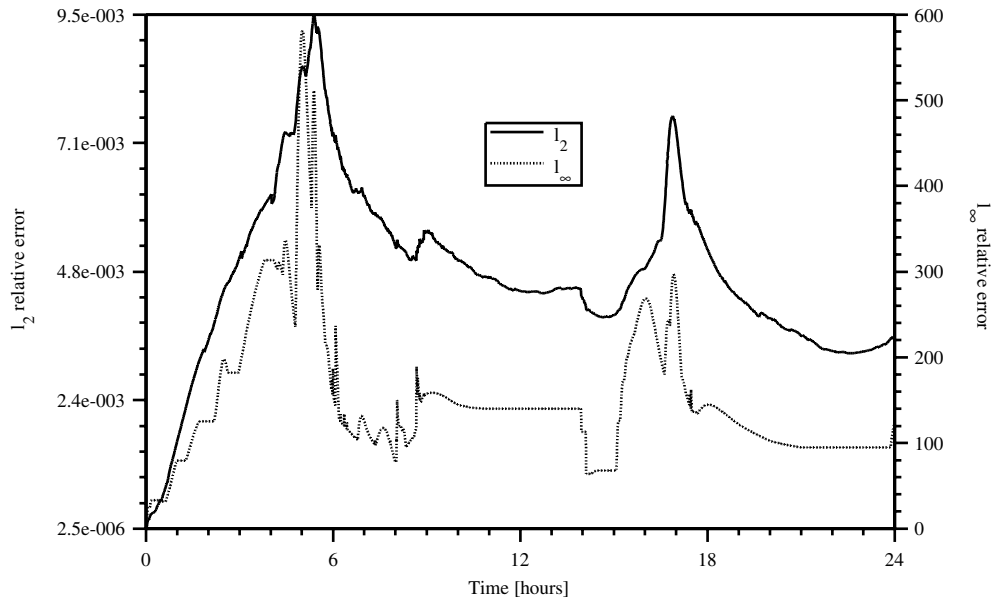


Figure 4. Relative errors for upwind non-CWC scheme 3 (incorrect Δz), test case with uniform initial datum.

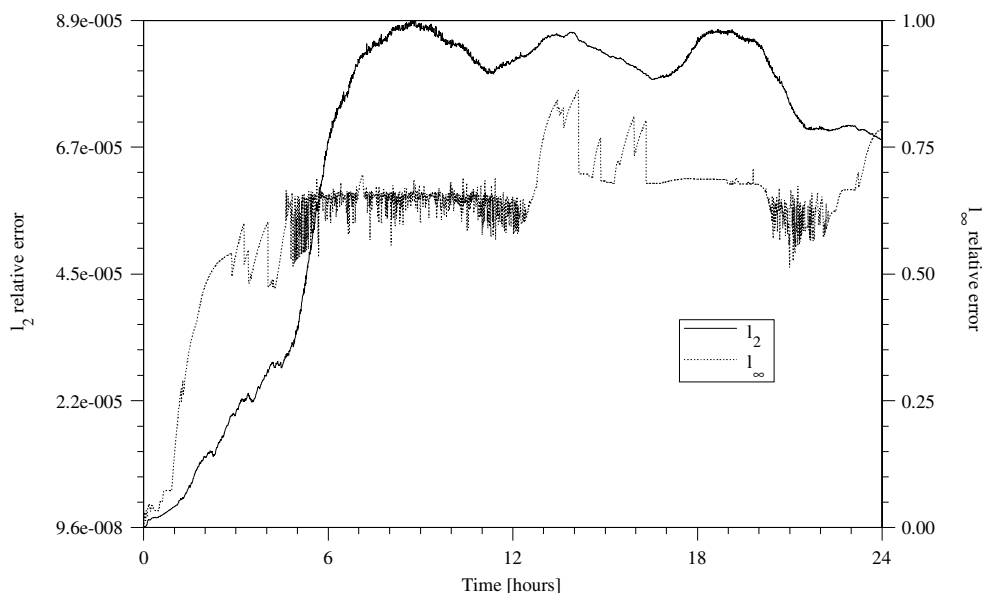


Figure 5. Relative errors for upwind non-CWC scheme 4 (incorrect velocity), test case with uniform initial datum.

machine accuracy. The errors in l_∞ , l_2 norm for the non-CWC upwind schemes 3 and 4 are reported in Figures 4 and 5, respectively. The error is particularly large in the case of upwind definition of the flux (SH): this happens because, in domains with complicated geometry like the Venice lagoon, the inconsistency between the conservative and the advective water flux mainly depends on the water depth H . It is clear that inconsistent schemes lead to errors that are unacceptable for practical application.

Realistic three-dimensional simulations of pointwise discharge of pollutant in the lagoon have then been performed. In this case, the vertical advection was discretized by the implicit upwind scheme in order to avoid heavy time-step restrictions. In order to test the longer term influence of CWC violations, a 10 day long simulation was run. For the vertical discretization, 28 layers of 1 m thickness were employed. The time step chosen for the hydrodynamic computation was 900 s, and substepping was used for passive tracer advection in order to comply with the Courant–Friedrichs–Lewy stability restriction. The errors, in l_∞ , l_2 norm for the non-CWC upwind schemes 3 and 4 are reported in Figures 6 and 7, respectively. In these case, the errors in l_∞ norm are one order of magnitude smaller than in the case with uniform concentration, while the l_2 errors are almost three orders of magnitude larger than in the uniform case. This shows that, in the non-uniform case, the error is more diffused and significantly affects the overall results. It is important to notice that, also in this case, the order of magnitude of the errors remains the same throughout the simulation.

In Figure 8 the relative difference in l_∞ , l_2 norm between the solution computed by CWC upwind advection (scheme 1) and the solution computed by CWC multidimensional upwind advection (scheme 2) is shown. The differences between the solutions computed by the two schemes are rather small and remain of the same order of magnitude throughout the simulation.

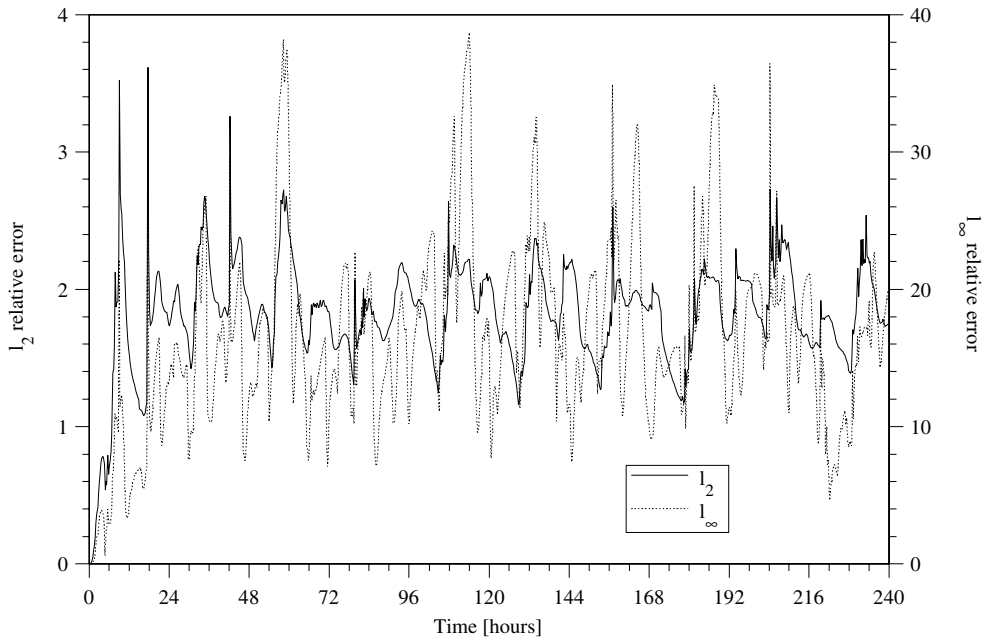


Figure 6. Relative errors for upwind non-CWC scheme 3 (incorrect Δz), test case with pointwise tracer discharge.

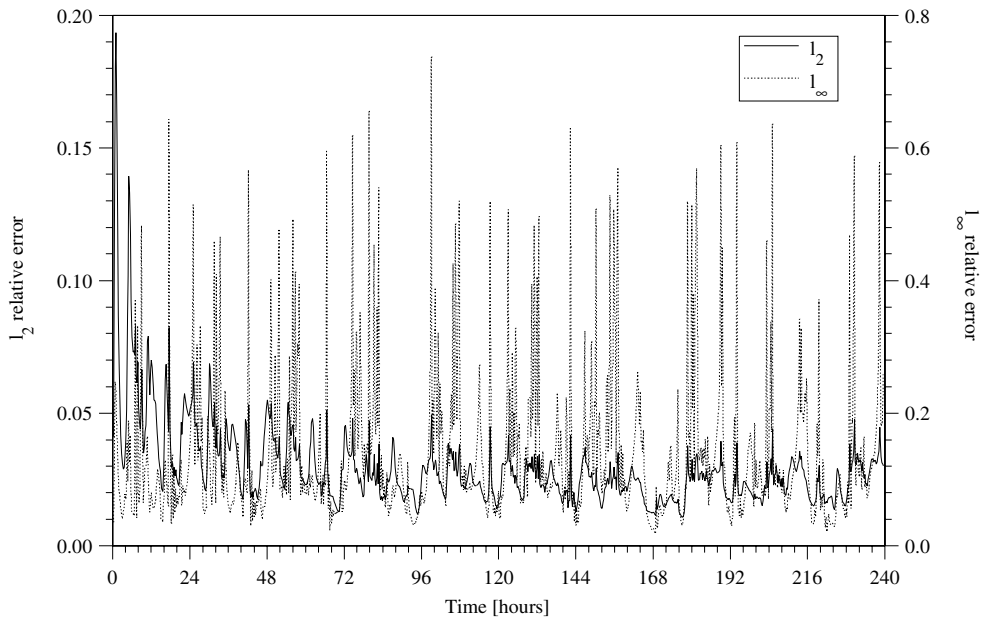


Figure 7. Relative errors for upwind non-CWC scheme 4 (incorrect velocity), test case with pointwise tracer discharge.

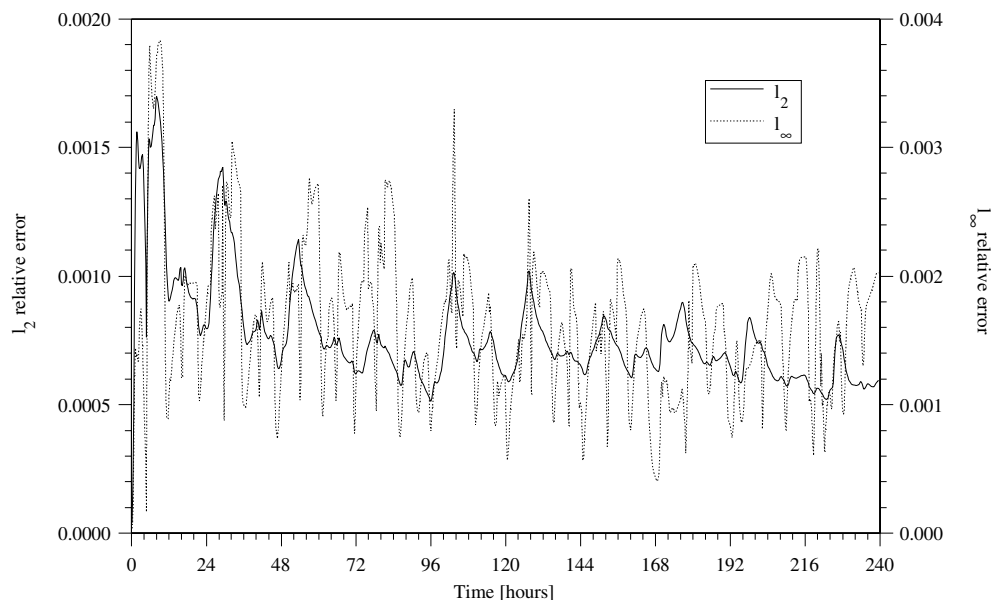


Figure 8. Relative difference between upwind-CWC scheme 1 and CTU-CWC scheme 2 solutions in test case with pointwise tracer discharge.

It can be assumed that they are mainly due to the difference in effective accuracy between the two schemes. The theoretically possible violations of the discrete maximum principle for the CTU scheme seem to play a negligible role in this type of practical applications.

9. CONCLUSIONS

In the framework of three-dimensional free-surface flows, consistency of discretization schemes for the scalar advection equation with the discretized continuity equation have been studied. The general form of a scheme consistent with the discretized continuity equation for the specific discretization employed in the very efficient and widely applied TRIM models has been presented. The role of this condition in proving monotonicity for upwind schemes in the free-surface context has been emphasized. Several numerical tests have been performed in order to display the errors that can be induced by the violation of the CWC condition. Both idealized and realistic tests show large errors and strongly non-monotonic behaviour in the results of schemes that do not satisfy the CWC condition.

ACKNOWLEDGEMENTS

We are greatly indebted to Vincenzo Casulli and Guus Stelling for many useful suggestions. Thanks are also due to Luigi Fraccarollo and Lisa Lucas for several useful comments.

REFERENCES

1. LeVeque R. *Numerical Methods for Conservation Laws*. Birkhäuser: Basel, 1990.
2. Toro EF. *Riemann Solvers and Numerical Methods for Fluid Dynamics*. Springer, 1997.
3. Goodman JB, LeVeque R. On the accuracy of stable schemes for 2D scalar conservation laws. *Mathematics of Computation* 1985; **45**:15–21.
4. Gross ES, Koseff JR, Monismith SG. Evaluation of advective schemes for estuarine salinity simulations. *ASCE Journal of Hydraulic Engineering* 1999; **125**:32–46.
5. LeVeque R. High resolution conservative algorithms for advection in incompressible flow. *SIAM Journal of Numerical Analysis* 1996; **33**:627–665.
6. Lin S, Rood RB. Multidimensional flux-form semi-Lagrangian transport schemes. *Monthly Weather Review* 1996; **119**:2046–2070.
7. Stelling GS, Kernkamp HWJ, Laguzzi MM. Delft flooding system: a powerful tool for inundation assessment based upon a positive flow simulation. *Hydroinformatics 98*, Babovic and Larsen (eds), Balkema, 1998.
8. Liu XD. A maximum principle satisfying modification of triangle based adaptive stencils for the solution of scalar hyperbolic conservation laws. *SIAM Journal of Numerical Analysis* 1993; **30**(3):701–716.
9. Casulli V. Semi-implicit finite difference methods for the two-dimensional shallow water equations. *Journal of Computational Physics* 1990; **86**(1):56–74.
10. Casulli V, Cattani E. Stability, accuracy and efficiency of a semi-implicit method for three-dimensional shallow water flow. *Computers and Mathematics with Applications* 1994; **27**:99–112.
11. Gross ES, Casulli V, Bonaventura L, Koseff JR. A semi-implicit method for vertical transport in multidimensional models. *International Journal for Numerical Methods in Fluids* 1998; **28**:157–186.
12. Gross ES, Koseff JR, Monismith SG. Three-dimensional salinity simulations of south San Francisco Bay. *ASCE Journal of Hydraulic Engineering* 1999; **125**:1199–1209.
13. Casulli V. A semi-implicit finite difference method for nonhydrostatic, free surface flow. *International Journal for Numerical Methods in Fluids* 1999; **30**:425–440.
14. Casulli V, Walters RA. An unstructured grid, three-dimensional model based on the shallow water equations. *International Journal for Numerical Methods in Fluids* 2000; **32**:331–348.
15. Colella P. Multidimensional upwind methods for hyperbolic conservation laws. *Journal of Computational Physics* 1990; **87**:171–200.
16. Toro EF. Riemann problems and the WAF method for the two-dimensional shallow water equations. *Philosophical Transactions of the Royal Society of London* 1992; **A341**:499–530.
17. Thacker WC. Exact solutions to the nonlinear shallow-water wave equations. *Journal of Fluid Mechanics* 1981; **107**:499–508.
18. Leonard BP, Lock AP, MacVean MK. Conservative explicit unrestricted-time step multidimensional constancy-preserving advection schemes. *Monthly Weather Review* 1996; **124**:2588–2606.